Cellulose (2014) 21:3371–3382
DOI 10.1007/s10570-014-0340-1

ORIGINAL PAPER

In situ synthesis of Ag_3PO_4/cellulose nanocomposites with photocatalytic activities under sunlight

Qiyang Wang · Jie Cai · Lina Zhang

Received: 30 January 2014 / Accepted: 20 June 2014 / Published online: 15 July 2014

Abstract In this work, we developed a strategy for Ag_3PO_4/cellulose nanocomposite hydrogels via in situ reduction and oxidation of Ag_3PO_4 nanoparticles in a cellulose matrix. The results of FT-IR, X-ray diffraction and X-ray photoelectron spectroscopy proved that the Ag_3PO_4 nanoparticles were successfully synthesized in situ in the cellulose hydrogels. Moreover, scanning electron microscopy and transmission electron microscopy indicated that various Ag_3PO_4 nanoparticles were synthesized, and they were dispersed uniformly in the regenerated cellulose hydrogels without aggregation with an average diameter of Ag_3PO_4 particles from 3.1 ± 2.7 to 11 ± 4.5 nm with an increase in Ag ion concentration. The photocatalytic degradation test of Ag_3PO_4/cellulose nanocomposite hydrogels provided evidence for the excellent photocatalytic degradation activity to rhodamine B under natural sunlight. Moreover, the photocatalytic degradation efficient increased with increasing Ag_3PO_4 concentration, where the decreasing of the Ag_3PO_4 nanoparticle size could increase the photocatalytic degradation speed. The porous structure of the cellulose hydrogels supplied not only cavities for the formation of Ag_3PO_4 nanoparticles, but also a shell to protect their nanostructure. The Ag_3PO_4/cellulose nanocomposite hydrogels exhibited good mechanical properties and thermal stability. This portable photocatalyst has good potential for application in the field of water pollution treatment.

Keywords Ag_3PO_4 nanoparticle · Cellulose hydrogel · In situ synthesis · Portable photocatalyst · Nanocomposite

Q. Wang · J. Cai (✉) · L. Zhang (✉)
Department of Chemistry, Wuhan University, Wuhan 430072, China
e-mail: jiecaiwhu@hotmail.com

L. Zhang
e-mail: zhangln@whu.edu.cn

Introduction

Semiconductor-based photocatalysis is a promising candidate for various applications in environmental pollution mediation and solar energy conversion (Hoffmann et al. 1995; Asahi et al. 2001; Maeda et al. 2006; Tokunaga et al. 2001; Tsuji et al. 2005; Khan et al. 2002) due to its photocatalytic activity and excellent physical and chemical properties (Mor et al. 2006; O'regan and Grfitzeli 1991; Han et al. 2011). However, titanium dioxide (TiO_2) has a wide band energy (3.2 eV) and small UV fraction (ca. 4 %) of the solar light used in photocatalysis (Chen et al. 2010). Being confronted with organic pollutants and the energy crisis, the development of semiconductor-based photocatalysis with a high level of activity under visible or solar light is a major topic. In recent years, several visible light-driven photocatalytic semiconductors such as $TiO_{2-x}N_x$ (Asahi et al. 2001), $CaBi_2O_4$

(Tang et al. 2004), $BiVO_4$ (Kudo et al. 1998) and Silver orthophosphate (Ag_3PO_4) have been reported. Among them, Ag_3PO_4 is a new type of photocatalyst with a body-centered cubic structure, possessing an excellent photocatalytic activity to decompose organic pollution because of the highly dispersive band structure (Yi et al. 2010; Bi et al. 2011; Ge et al. 2012). Moreover, the size of Ag_3PO_4 remains relatively large, which might have an effect on the photcatalytic activity (Dinh et al. 2011). The higher surface area of smaller particle size is thought to be of benefit to the photocatalytic reaction, which mostly occurs on the catalyst surface (Linsebigler et al. 1995). To enhance the photocatalytic activity of Ag_3PO_4, construction of Ag_3PO_4 nanoparticles with highly uniform size is also an efficacious method to remove contaminants in solution. However, it is very difficult to remove nanoparticles from solutions, and this may cause secondary pollution to the environment. To solve this problem, hybridization of nanoparticles with renewable biomass macromolecules such as cellulose and chitin has been very impressive (Sehaqui et al. 2010; Caruso and Schattka 2000; Murray et al. 2005).

Cellulose is the most abundant and renewable natural polymer on earth as well as one of the raw materials for agriculture and industry. However, cellulose is the most intransigent macromolecule, being difficult to dissolve. In our laboratory, 4.6 wt% LiOH/15 wt% urea and 7 wt% NaOH/12 wt% urea aqueous solution precooled to −12 °C were developed to dissolve cellulose and yield a transparent cellulose solution (Cai et al. 2008b). Moreover, from the cellulose solution, regenerated cellulose hydrogels (Chang et al. 2009, a, b), films, fibers (Cai et al. 2007) and cellulose-based nanocomposites (Cai et al. 2012; Qi et al. 2009; Cai et al. 2008a; Liu et al. 2008; Dankovich and Gray 2011) have been fabricated, showing remarkable mechanical, optical and thermal properties. The portable photocatalyst using hydrogel as a matrix was conducive to water penetration and could be very efficient in degrading organic pollution. Therefore, photocatalyst/cellulose hydrogels were constructed for use in water treatment of organic pollution. In this article, we developed a strategy for cellulose-inorganic hybridization via in-suit reduction and oxidation to fabricate Ag_3PO_4 nanoparticles in regenerated cellulose hydrogels. The cellulose-based nanocomposites with finely distributed nanoparticles of Ag_3PO_4 were fabricated to achieve a maximum Ag_3PO_4 loading of about 26 %. Moreover, the Ag_3PO_4/cellulose nanocomposites as photocatalysts of decomposing organic dye (Rh B) under natural sunlight were evaluated. Our findings may provide a new and facile pathway for fabricating photocatalytic materials to solve the problem of organic pollution under natural sunlight and expand the application of cellulose.

Experimental section

Materials

Cotton linter pulp with an α-cellulose content of more than 95 % was provided by Hubei Chemical Fiber Co.n Ltd., China. Its viscosity-average molecular weight (M_η) was determined to be 9.8×10^4 (Cai et al. 2006) by viscometry at 25 ± 0.05 °C in aqueous 4.6 wt% LiOH/15.0 wt% urea solution. Urea, $LiOH{\cdot}H_2O$, silver nitrate ($AgNO_3$), 30 % hydrogen peroxide (H_2O_2) and other reagents were purchased from Hubei ShengShi Chemical Reagent Co., Ltd.

Preparation of regenerated cellulose hydrogels

The 4.6 wt% LiOH/15.0 wt% urea aqueous solution was precooled to −12 °C, and the desired amount of cellulose pulp was immediately dispersed and stirred to obtain a transparent cellulose solution with 4 wt% concentration. The cellulose solution was subjected to centrifugation at 5,000 rpm for 15 min at 5 °C in order to carry out the degasification. The resulting transparent solution was cast on a glass plate to give a thickness of 0.5 mm and then immersed in a nonsolvent solution (5 wt% H_2SO_4 solution) for the desired time to form regenerated cellulose gel (RC). Regenerated cellulose gel film was washed thoroughly with deionized water to obtain cellulose hydrogel.

Preparation of Ag_3PO_4/cellulose composite hydrogel (SP)

The hydrothermal reduction of $AgNO_3$ by cellulose was performed by immersing the regenerated cellulose hydrogel into $AgNO_3$ aqueous solution at 80 °C for 24 h. The $AgNO_3$ concentration was 0.05, 0.1 and 0.4 mol/l, respectively. Then, the cellulose hydrogels containing Ag nanoparticles were washed with

deionized water and dipped into 0.2 M Na_2HPO_4/200 ml 30 % H_2O_2 solution for 0.5 h at room temperature to transform Ag_3PO_4. The resultant Ag_3PO_4/cellulose composite hydrogels were rinsed with deionized water for three times before using. The Ag_3PO_4/cellulose composite hydrogels prepared from $AgNO_3$ solution with concentrations of 0.05, 0.1 and 0.4 mol/l were coded as SP05, SP10 and SP40, respectively. The aerogel samples were prepared by freeze-drying from the hydrogels for the measurement of SEM and X-ray diffraction (XRD).

Characterization

Scanning electron microscopy (SEM) observation was carried out on an FE-SEM (SIRION TMP, FEI) by using an accelerating voltage of 12 kV. The samples were coated with Pt for the SEM observation. Transmission electron microscopy (TEM) was observed on a JEOL JEM-2100 at an accelerating voltage of 200 kV. The samples were embedded using resin, and ultrathin sectioning was placed with a copper line. Attenuated total reflection Fourier transform infrared (ATR-FTIR) spectroscopy was measured on an FT-IR spectroscopy (model 1600, PerkinElmer Co., USA). Samples were cut into powder and dried in an oven at 60 °C for 24 h. X-ray diffraction (XRD) measurement was taken on an XRD diffractometer (D8-Advance, Bruker, USA) in a symmetric reflection mode. The patterns with Cu Kα radiation ($\lambda = 0.15406$ nm) at 40 kV and 40 mA were recorded in the 2θ range of 8 to 90°. All samples were cut into powder to remove the influence of the crystalline orientation. The crystallite size (D) of the sample for the (210) plane of Ag_3PO_4 nanoparticle was calculated by the Scherrer formula(Patterson 1939):

$$D = 0.9\lambda/(\beta \cdot \cos\theta) \quad (1)$$

where $\lambda = 0.15406$ nm, β is the corrected integral width, and θ is the Bragg angle. X-ray photoelectron spectroscopy (XPS) was recorded on an XSAM 800 Instrument (Kratos, UK). An MgKa target at 1,253.6 eV and 16 mA × 12.5 kv was used in the experiment. Regular light absorbance was measured at wavelengths from 200 to 800 nm using a UV-visible spectrometer (U-4100, Hitachi High-Technologies Corp.). The photocatalytic activities of Ag_3PO_4/cellulose nanocomposite hydrogel were tested by using a rhodamine B (Rh B) aqueous solution. A piece of (6.4 cm × 2.6 cm × 0.5 cm) Ag_3PO_4/cellulose nanocomposite hydrogel was immersed into Rh B aqueous solution (100 ml, 0.01 g/L) for 8 h in the dark. Then the Rh B aqueous solution including the sample was illuminated under sunlight. The change in the Rh B concentration was monitored using a UV-vis spectrophotometer at a wavelength of 552 nm. Thermal gravimetric analysis (TGA) was carried out by a Netzsch thermogravimetric analyzer (STA449C, 31MFC, G Jupiter, German). The dry samples were cut into powder in a crucible and heated from 30 to 600 °C at a heating rate of 10 K/min in nitrogen and air atmosphere, respectively. Tensile tests of the Ag_3PO_4/cellulose composite hydrogels were performed using a universal testing machine (CMT6503, Shenzhen SANS Test Machine Co., Ltd., Shenzhen, China) with a tensile rate of 5 mm min^{-1} to obtain tensile strength (σ_b) and elongation at break (ε_b). Rectangular-shaped specimen strips were 5 mm in length and 0.5 mm in width. Densities of the samples were calculated by weighing the samples and measuring the volumes.

Results and discussions

Evidence of Ag_3PO_4 nanoparticles immobilized in the cellulose matrix

Figure 1a shows a schematic illustration for the preparation of the Ag_3PO_4/cellulose nanocomposites. Silver ions can be reduced to silver nanoparticle by hydroxyl groups of cellulose and reducing end groups (Kotel'nikova et al. 2003). Moreover silver nanoparticles were dispersed in cellulose matrix, and the size of the silver nanoparticles could also be controlled in the pore. When the cellulose hydrogel films were immersed into $AgNO_3$ aqueous solution, Ag^+ ions were tightly stabilized in the cellulose hydrogel by interacting with –OH groups of the cellulose hydrogel because of electrostatic interactions (Cai et al. 2008a; Liu et al. 2011a). Subsequently, the cellulose hydrogel with $AgNO_3$ was heated. Ag ions were reduced by cellulose end aldehyde and alcohol groups, and Ag nanoparticels were stabilized in cellulose hydrogels. By using the oxidation ability of H_2O_2, Ag nanoparticles were transformed into Ag_3PO_4 nanoparticles by the reaction of Ag and HPO_4^{2-}. Hydrogen peroxide of cellulose can oxidize Ag particle to Ag^+ ions (Wang

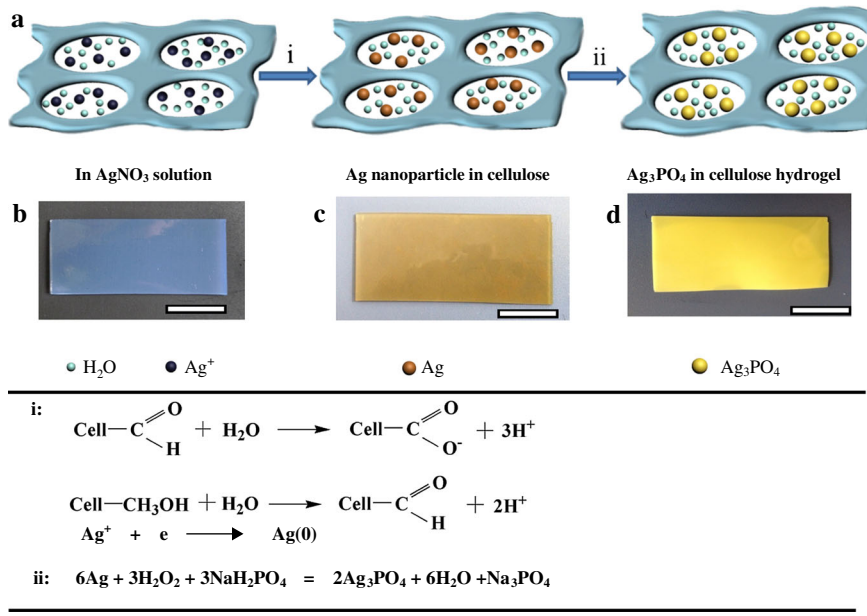

Fig. 1 Schematic illustration of the fabrication of Ag_3PO_4 nanoparticles in the cellulose hydrogel film (**a**, *i* Ag ions were reduced to Ag nanoparticle by cellulose at 80 °C; *ii* Ag_3PO_4 nanoparticles were fabricated in NaH_2PO_4 of 30 % H_2O_2 solution.) and the photograps of cellulose hydrogel (**b**), Ag/cellulose composite (**c**) and Ag_3PO_4/cellulose nanocomposite (**d**). (The *scale bar* is 2 cm)

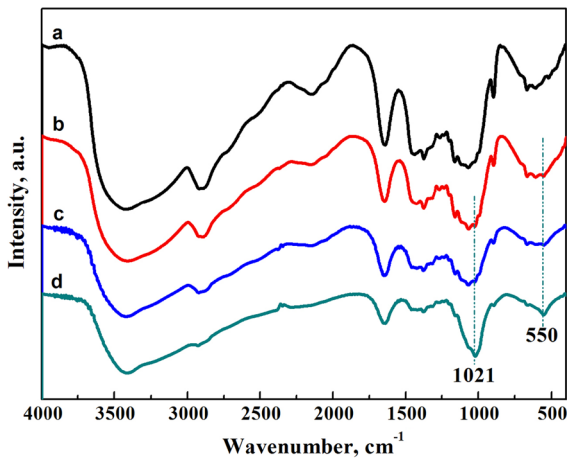

Fig. 2 FT-IR spectra of RC (*a*) and Ag_3PO_4/cellulose nanocomposite hydrogels (*b* SP05, *c* SP10, *d* SP40)

et al. 2012). When H_2O_2 has been introduced, the redox potential of H_2O_2/H_2O ($E^{\theta} = +1.776$ V) was higher than that of Ag_3PO_4/Ag ($E^{\theta} = +0.451$ V) (Hu et al. 2013). Thus, the color of cellulose hydrogels (b) was transformed into a brown color (c) after hydrothermal reduction in $AgNO_3$ solution and then immediately changed to yellow (d) when cellulose hydrogels were immersed into Na_2HPO_4 hydrogen peroxide solution, indicating the formation of Ag_3PO_4 nanoparticles.

FT-IR spectra of RC and SP05, SP10, SP40 are shown in Fig. 2. The peak at 3,420 cm^{-1} is attributed to hydroxyl group (OH) stretching vibrations of cellulose in the composites. A broad peak at around 3,400 cm^{-1} corresponds to a large number of hydroxyl groups in the Ag_3PO_4 nanoparticle surface (Chen et al. 2007; Nguyen et al. 2009). The results indicated that Ag_3PO_4 nanoparticles retained the intermolecular hydrogen bond in the cellulose hydrogels. The two peaks at 1,021 and 550 cm^{-1} corresponded to P–O stretching vibrations of PO_4^{3-} ions (Thomas et al. 2002). This confirmed that the Ag^+ ions existed in the Ag_3PO_4 form in the composite hydrogels.

The X-ray photoelectron spectroscopy (XPS) was carried out to investigate the surface composition and chemical state of the composite hydrogels. Figure 3 shows the XPS spectra for the Ag_3PO_4/cellulose composite hydrogel (SP10). The C1s spectra of the Ag_3PO_4/cellulose nanocomposite are shown in Fig. 3a. There is an individual peak at 286.3 eV attributed to the C–O bond of cellulose (Belgacem

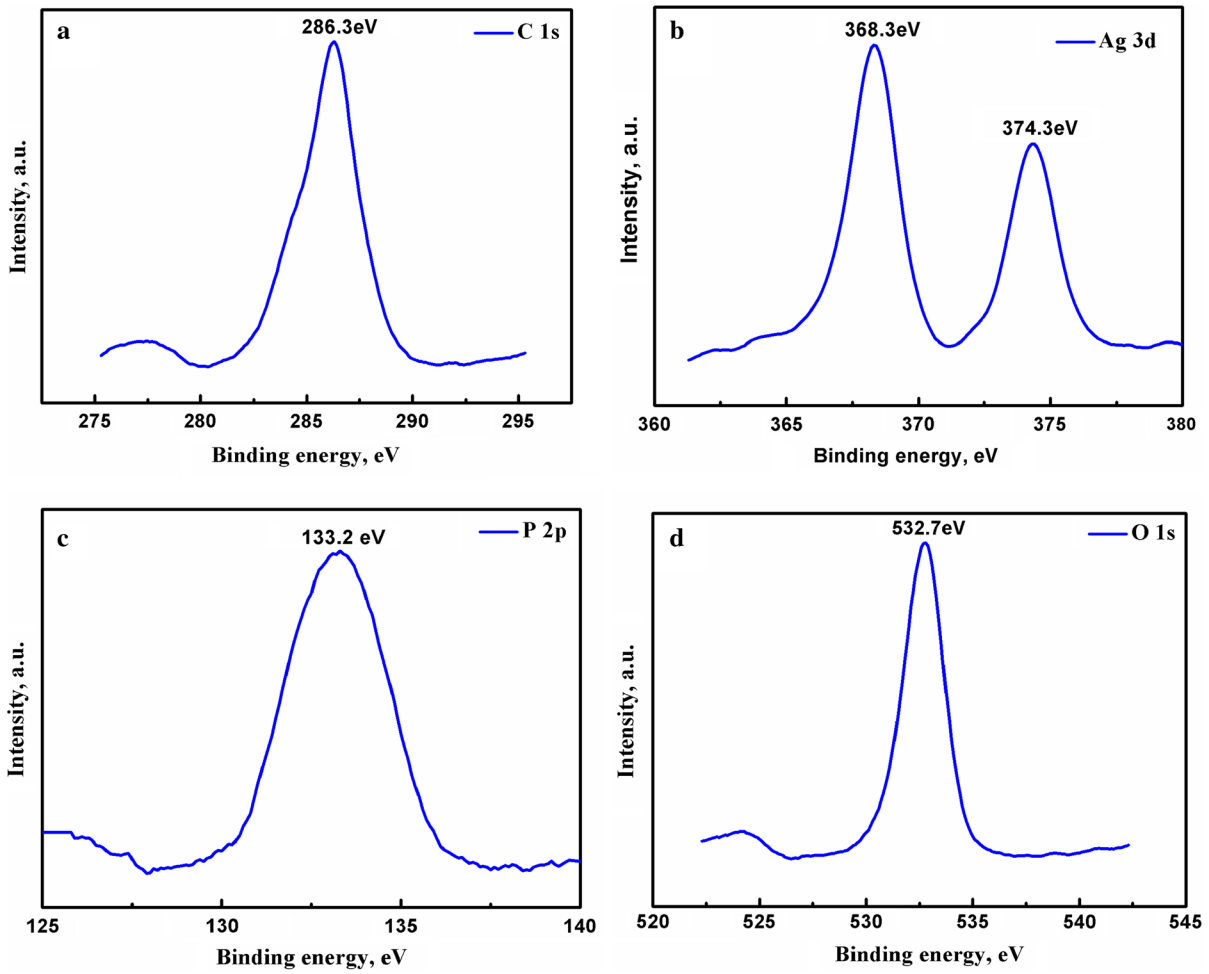

Fig. 3 The XPS spectra for the Ag_3PO_4/cellulose nanocomposite hydrogel (SP10)

et al. 1995). The peaks at the binding energy of 374.3 and 368.3 eV are attributed to Ag3$d_{3/2}$ and Ag3$d_{5/2}$ binding energies (Ge et al. 2012; Zhang et al. 2008; Murray et al. 2005; Chen et al. 2006). The peaks at 133.2 and 532.7 eV correspond to the P^{5+} and O^{2-} anion (Zheng et al. 2008; Yang et al. 2009; Zhao et al. 2009). The results from XPS indicated that the Ag_3PO_4 nanoparticles were successfully synthesized in situ in the cellulose hydrogels.

The morphology of the cellulose and Ag_3PO_4/cellulose composite hydrogels were observed by SEM. The SEM images of the RC hydrogel and Ag_3PO_4/cellulose composite hydrogels are shown in Fig. 4. The RC hydrogels display a micro- and nanoporous structure, which was caused by the phase separation of the cellulose solution during the regenerating process. The SEM images of the Ag_3PO_4/cellulose composite hydrogels in Fig. 4b–d displayed that the Ag_3PO_4 nanoparticles were embedded in the cellulose matrix and were filled into the pore of the cellulose hydrogels. Clearly, the Ag_3PO_4 nanoparticles were uniformly distributed in the cellulose matrix. As shown in Fig. 4, the composite hydrogels of SP05, SP10 and SP40 exhibited a relatively denser surface than those of RC. It was confirmed that Ag_3PO_4 particles were synthesized in situ in the cellulose hydrogel and tightly hybridized with a cellulose backbone via hydrogen bond and electrostatic interactions. The porous structure of the cellulose hydrogels supplied not only cavities for the formation of the Ag_3PO_4 nanoparticles, but also a shell to protect their nanostructure.

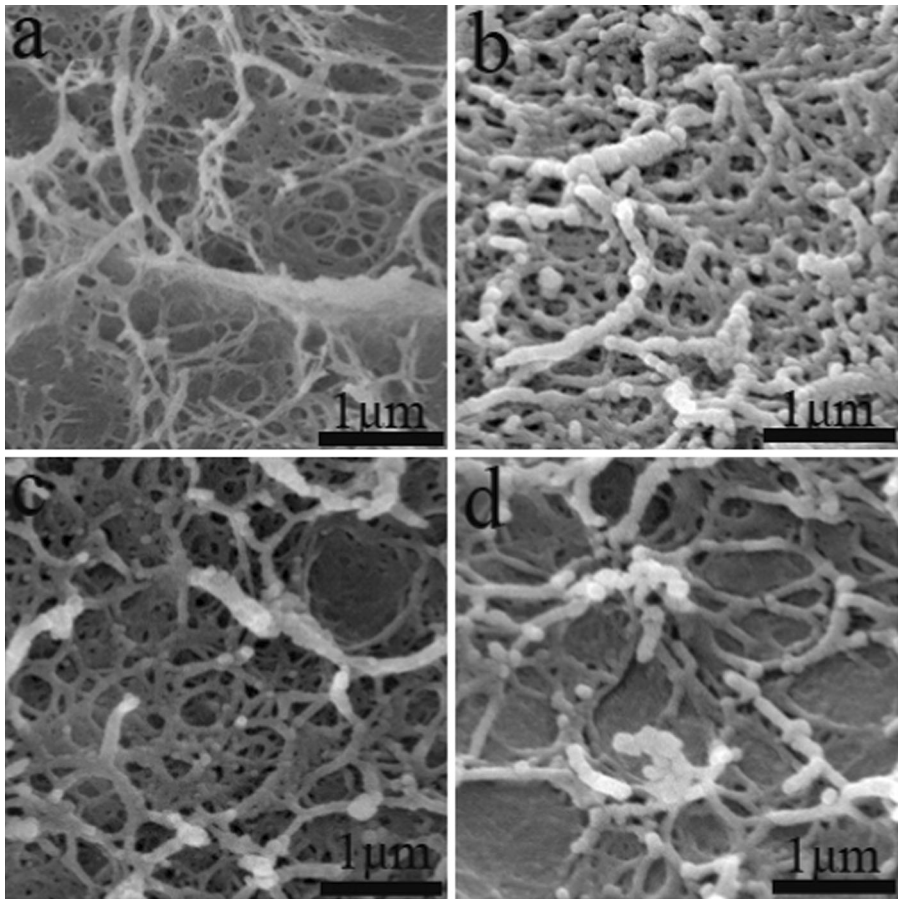

Fig. 4 The SEM images of cellulose hydrogel (RC) (**a**) and Ag_3PO_4/cellulose nanocomposites SP05 (**b**), SP10 (**c**) and SP40 (**d**)

Figure 5 shows the TEM images of the Ag_3PO_4/cellulose composites and size histograms of the Ag_3PO_4 nanoparticles. As expected, Ag_3PO_4 nanoparticles at each $AgNO_3$ concentration were synthesized and dispersed uniformly in the regenerated cellulose hydrogels without aggregation. The size histograms showed that the average diameter of the Ag_3PO_4 particle of SP05, SP10 and SP40 increased gradually from 3.1 ± 2.7 to 11 ± 4.5 nm with an increase in $AgNO_3$ concentration. It has been reported that the growth and aggregation of nanoparticles can be controlled in cellulose hydrogel because the pores of the cellulose matrix can limit the growth of the nanoparticles (Luo et al. 2009; Pinto et al. 2008; Yu et al. 2012). Therefore, the microporous nature of cellulose hydrogels could play an important role in the in situ synthesis, dispersion and stabilization of Ag_3PO_4 inorganic nanoparticles.

The X-ray diffraction (XRD) patterns of RC, SP05, SP10 and SP40 are shown in Fig. 6. There are two peaks of RC at $2\theta = 12.2°$, $20.2°$, corresponding to the $(1\bar{1}0)$, (110) crystal plane of cellulose II crystalline (Isogai et al. 1989). However, the X-ray diffraction patterns of SP05, SP10 and SP40 clearly showed that all peaks of the samples are a near-systematic superposition of those of pure cellulose and body-centered cubic structure of Ag_3PO_4 (JCPDS card no. 060505) (Yi et al. 2010). The peak intensity of Ag_3PO_4 intensified with the enhancement of the $AgNO_3$ solution concentrations, which is a sign of the increasing of Ag_3PO_4 amounts in the composite hydrogels. The average crystal size of Ag_3PO_4 nano-

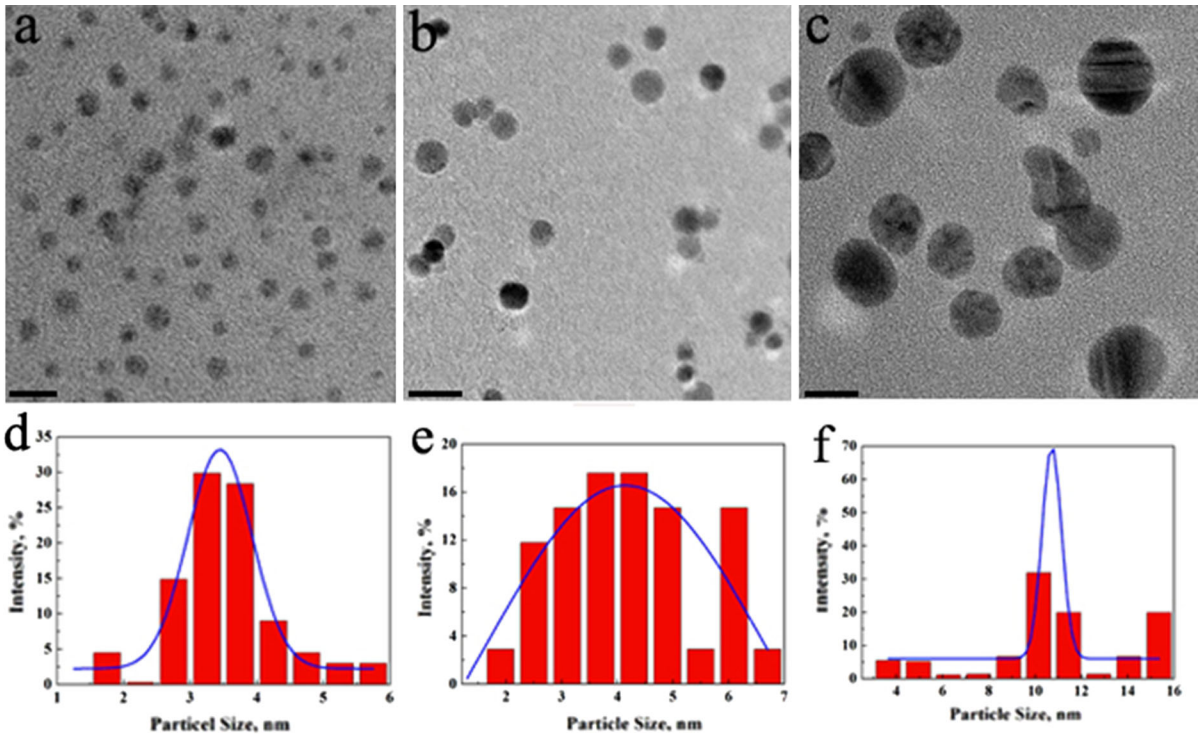

Fig. 5 HRTEM images (**a**, **b**, **c**) and particle size histograms (**d**, **e**, **f**) of Ag_3PO_4 nanoparticles corresponding to **a**-**c**. (All scale bars are 10 nm)

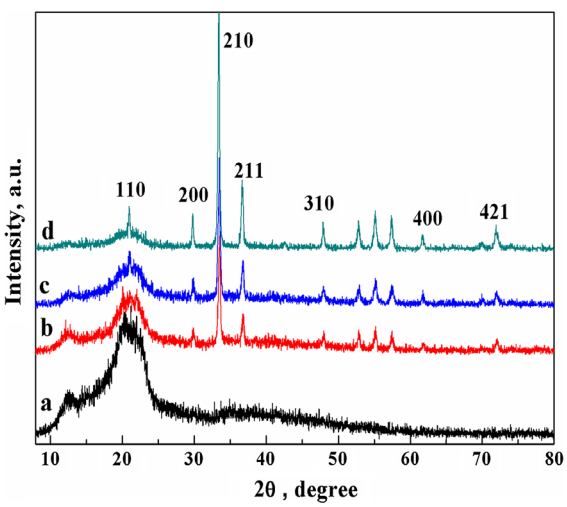

Fig. 6 XRD patterns of the RC (*a*), SP05 (*b*), SP10 (*c*) and SP40 (*d*), respectively

particles for SP05, SP10 and SP40 obtained using Scherrer's formula (Formula 1) was 12.9, 15.5 and 19.3 nm, respectively. Therefore, the Ag_3PO_4 nanoparticles were successfully constructed via a facile and simple pathway, leading to the conformation of inorganic/cellulose composite materials.

Photocatalytic properties of Ag_3PO_4/cellulose composite under sunlight

Figure 7 shows the UV-visible spectra of Ag_3PO_4/cellulose composite (SP05, SP10 and SP40). The results indicated that the Ag_3PO_4/cellulose composites (SP05, SP10, SP40) can absorb energy with a wavelength shorter than $\backsim$530 nm. Moreover, the absorption peak edge of the Ag_3PO_4/cellulose nanocomposite hydrogels shifted to higher wavelength with the increasing of Ag_3PO_4 concentration. The band gap (E_g) of the semiconductor can be obtained from the equation below (Kim et al. 2008):

$$\alpha h\nu = k(h\nu - E_g)^{n/2} \quad (2)$$

where α, ν and k are the adsorption coefficient, light frequency and proportionality constant, respectively. Figure 7b shows the curves of $(\alpha h\nu)^2$ versus $h\nu$ for a

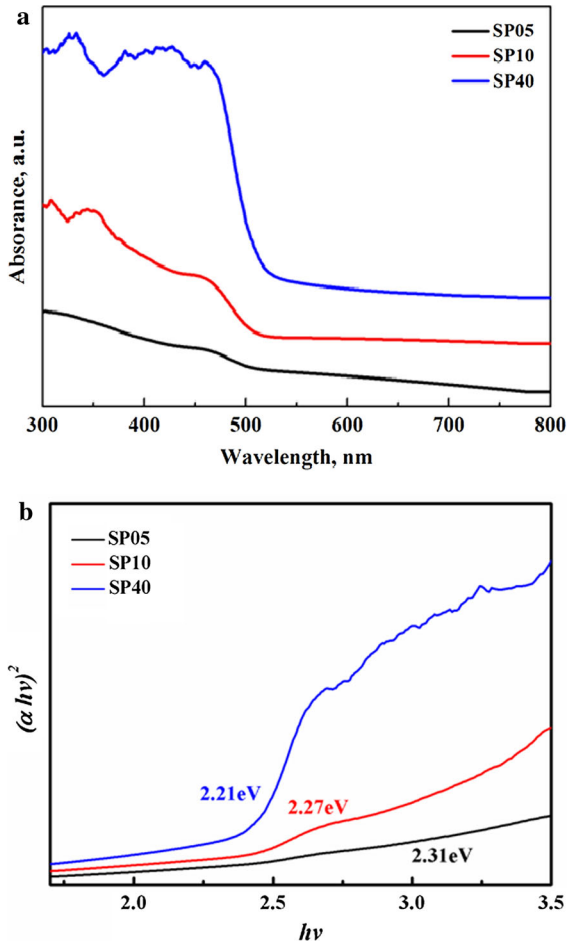

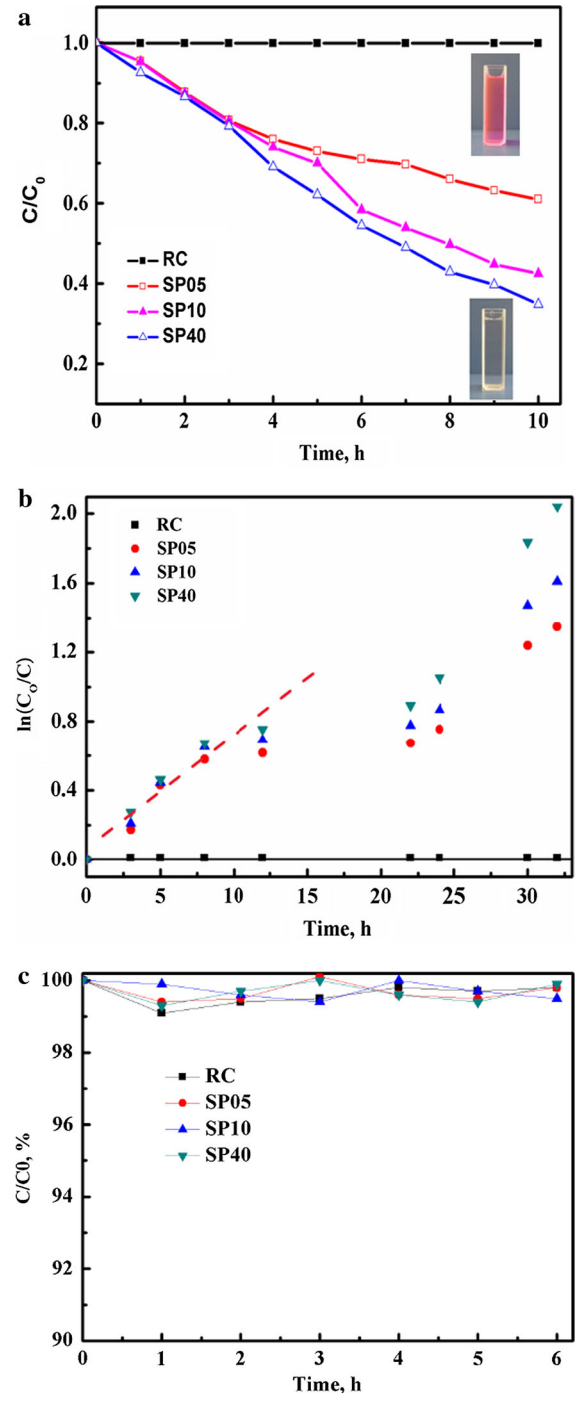

Fig. 7 The UV-vis spectrum (**a**) of Ag_3PO_4/cellulose composites (SP05, SP10, SP40) and the plot of $(\alpha hv)^2$ versus *hv* (*bottom*) for the direct transition as a function of photon energy (**b**)

direct transition with *n* equal to 1. The direct band gap fit of the absorption edges were calculated to be 2.21, 2.27 and 2.31 eV for SP05, SP10 and SP40, respectively. It was not difficult to imagine that the Ag_3PO_4 nanoparticles in the cellulose hydrogel had a good photocatalytic ability as a result of an increase in the apparent bandgap energy.

To prove the narrower band gap to enhance photon energy utilization for comparison, the photocatalytic degradation of Rh B solution by Ag_3PO_4/cellulose hydrogels was evaluated under natural sunlight at room temperature. As shown in Fig. 8, all of the nanocomposite hydrogels exhibited good photocatalytic activities for the Rh B degradation reaction under sunlight. The concentration of the Ag_3PO_4 nanoparticles of all samples for photodegradation of the Rh B aqueous solution (0.1 g/l) was about 0.54, 1.4 and 3.55 mg/ml, respectively. It was noted that the photocatalytic activity of the sample (SP40) under sunlight was higher than that of SP10 and SP05. It was noted that SP40 decomposed 50 % Rh B aqueous

◀**Fig. 8** **a** Photodegradation of RhB over the cellulose hydrogel (RC) and Ag_3PO_4/cellulose nanocomposites (SP05, SP10, SP40) under natural sunlight. The inset photographs show the color changes of Rh B solution corresponding to the SP40. **b** The relationship between $\ln(C/C_0)$ and reaction time with different concentrations of Ag_3PO_4. **c** Photodegradation of Rh B over the cellulose hydrogel (RC) and Ag_3PO_4/cellulose nanocomposites (SP05, SP10, SP40) at night and without light

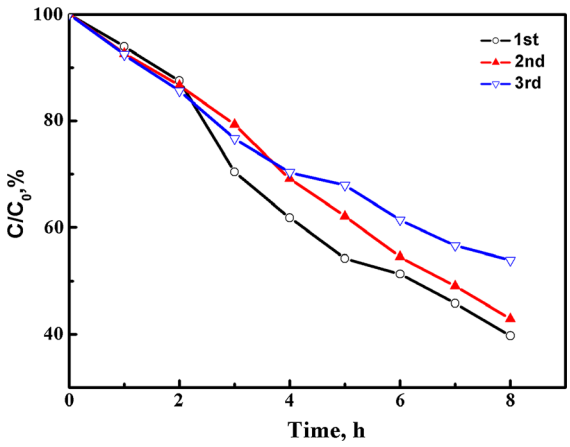

Fig. 9 Cyclic photodegradation curves of Rh B with the SP40 composites

solution within about 6.5 h under sunlight, whereas the other hyhdrogels (SP05, SP10) needed more time. This could result from the relatively high Ag_3PO_4 concentration of SP40. However, if we consider the degradation rate per unit mass of the Ag_3PO_4 particles, SP05 should possess higher degradation efficiency. Namely, the nanoparticle size was smaller and the degradation efficiency higher. Figure 8b shows the relationship between $\ln(C/C_0)$ and reaction time with different Ag_3PO_4 concentrations. As shown in Fig. 8b, SP05 had a higher degradation efficiency. Therefore, it was suggested that the narrower band gap benefited enhanced photon energy utilization. Moreover, in Fig. 8c, the Rh B aqueous solution did not change under dark. This indicated the establishment of an adsorption-desorption equilibrium without light.

The cyclic photogradation curves of Rh B by SP40 composite hydrogel under sunlight are shown in Fig. 9. The composite exhibited remarkable photostability almost without any loss of photocatalytic activity after three cycles. Namely, the photocatalytic activity of the composite hydrogel was very stable. The Ag_3PO_4/cellulose hydrogels with excellent mechanical properties, dimensional stability and reusability can be used as portable photocatalysts.

Thermal and mechanical properties of Ag_3PO_4/cellulose hydrogel

The satisfactory mechanical and thermal stability is essential for the successful application of the materials as a portable photocatalyst. The TGA and DTG curves for cellulose (RC) and Ag_3PO_4/cellulose nanocomposites (SP05, SP10, SP40) under air and nitrogen atmosphere are shown in Fig. 10. For TGA curves, the weight loss around 5 % below 150 °C resulted from the evaporation of absorbed water. The decomposition temperature of the cellulose was about 332 °C under air and nitrogen atmosphere, and the cellulose completely decomposed (about 100 %) at about 520 °C under air atmosphere and decomposed (about 80 %) at 600 °C under nitrogen atmosphere. Moreover, the decomposition temperature of nanocomposites shifted slightly to lower temperature in comparison with cellulose and shifted to lower temperature with increasing Ag_3PO_4 concentration under air and nitrogen atmosphere. Heating in air and nitrogen induced the decomposition of cellulose, with the first stage of the samples of SP05, SP10 and SP40 between 210 and 300 °C shifting slightly to lower temperature, probably because of the catalysis effect of Ag_3PO_4 particles. Moreover, the secondary stage of the sample decomposition appeared between 300 and 370 °C for SP05 and SP10, and the decomposition temperature of SP40 appeared between 300 and 600 °C. Importantly, the third stage of the samples of SP05 and SP10 appeared between 370 and 600 °C because of the burning of char (Liu et al. 2011b). Since the Ag_3PO_4 was relative stable, the Ag_3PO_4 content for SP05, SP10 and SP40 was estimated to be about 8, 16 and 26 wt%, respectively. In view of the above results, the thermal stability of the Ag_3PO_4/cellulose hydrogels was slightly lower than that of cellulose hydrogel, but the thermal resistance of composite hydrgels was better than that of the general synthetic plastic (Jeon et al. 2013; Soltani et al. 2013) and was sufficient for the application of portable photocatalyst.

Figure 11 shows the typical stress-strain curves of RC, SP05, SP10 and SP40. The result indicated that the tensile strength of Ag_3PO_4/cellulose composite hydrogels increased slightly with an increase in Ag_3PO_4 content as a result of the strong interactions

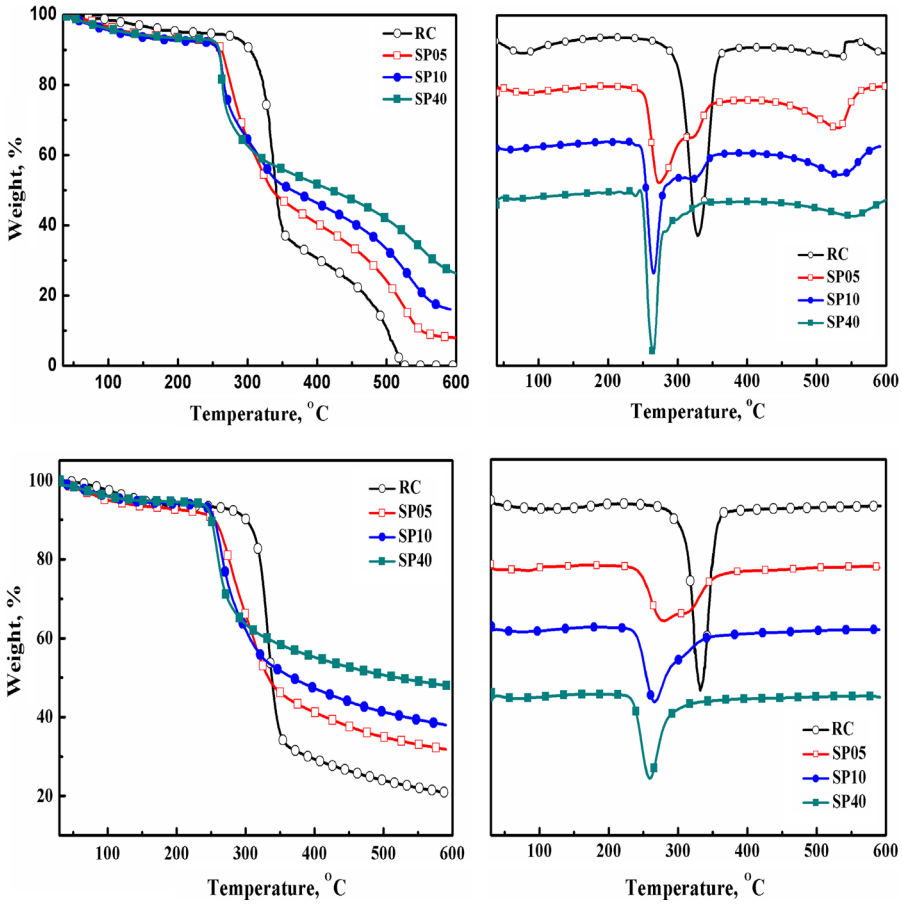

Fig. 10 TGA and DTG curves for RC, SP05, SP10 and SP40 under air (*top*) and nitrogen (*bottom*) atmosphere

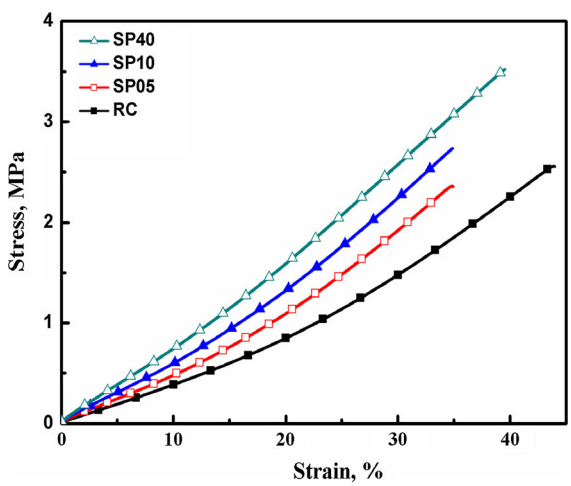

Fig. 11 Typical stress-strain curves of RC, SP05, SP10 and SP40 at wet state

between the Ag_3PO_4 particles and cellulose hydrogel. Moreover, the Young's modulus of Ag_3PO_4/cellulose composite hydrogels also increased slightly with increasing Ag_3PO_4 content, as determined by the rigidity of the inorganic nanoparticle. In our findings, the Ag_3PO_4 particles were tightly embedded in the cellulose hydrogel loading to enhance the mechanical properties of the composites. The physical properties of cellulose/Ag_3PO_4 are shown in Table 1. Therefore, the mechanical properties of portable photocatalytic hydrogel might be more excellent than those of general hydrogel (Nakayama et al. 2004; Xiang et al. 2006), and the portable photocatalytic hydrogels have a broader potential for photocatalytic application.

Conclusion

Ag_3PO_4/cellulose nanocomposite hydrogels were successfully synthesized in situ in two steps using the cellulose reduction itself and H_2O_2 oxidation capacity. The Ag_3PO_4 nanoparticles at different $AgNO_3$ concentrations were dispersed uniformly in the regenerated cellulose hydrogels, and their average diameter

Table 1 Mechanical properties of cellulose hydrogel and Ag_3PO_4/cellulose nanocomposite hydrogel

Samples	$AgNO_3$ concentration in aqueous (mol/l)	Ag_3PO_4 content (wt%)	Ag_3PO_4 particle size (d, nm)	Tensile strength (MPa)	Elongation at break (%)	Young's modulus (MPa)
RC	0	–	–	2.5	44	3.8
SP05	0.05	8	3.1 ± 2.7	2.4	35	5.0
SP10	0.1	16	4.1 ± 2.4	2.7	35	5.8
SP40	0.4	26	11 ± 4.5	3.5	40	7.3

was in the range of 3.1 ± 2.7 to 11 ± 4.5 nm and slightly increased with an increase in Ag_3PO_4 concentration. The Ag_3PO_4/cellulose nanocomposite hydrogels had good degradation efficiency in the photocatalytic degradation on Rh B, and the Ag_3PO_4 nanoparticle size was smaller and the degradation efficiency higher. The Ag_3PO_4/cellulose nanocomposite hydrogels exhibited excellent mechanical properties and moderate thermal stability. This material has the potential for application in the field of visible light photocatalytic water treatment and solar energy conversion.

Acknowledgments This work was supported by the National Basic Research Program of China (973 Program, 2010CB732203), the Major Program of the National Natural Science Foundation of China (21334005) and the National Natural Science Foundation of China (51373125 and 20904043).

References

Asahi R, Morikawa T, Ohwaki T, Aoki K, Taga Y (2001) Visible-light photocatalysis in nitrogen-doped titanium oxides. Science 293(5528):269–271

Belgacem M, Czeremuszkin G, Sapieha S, Gandini A (1995) Surface characterization of cellulose fibres by XPS and inverse gas chromatography. Cellulose 2(3):145–157

Bi Y, Ouyang S, Umezawa N, Cao J, Ye J (2011) Facet effect of single-crystalline Ag_3PO_4 sub-microcrystals on photocatalytic properties. J Am Chem Soc 133(17):6490–6492

Cai J, Liu Y, Zhang L (2006) Dilute solution properties of cellulose in LiOH/urea aqueous system. J Polym Sci, Part B: Polym Phys 44(21):3093–3101

Cai J, Zhang L, Zhou J, Qi H, Chen H, Kondo T, Chen X, Chu B (2007) Multifilament fibers based on dissolution of cellulose in NaOH/urea aqueous solution: structure and properties. Adv Mater 19(6):821–825

Cai J, Kimura S, Wada M, Kuga S (2008a) Nanoporous cellulose as metal nanoparticles support. Biomacromolecules 10(1):87–94

Cai J, Zhang L, Liu S, Liu Y, Xu X, Chen X, Chu B, Guo X, Xu J, Cheng H (2008b) Dynamic self-assembly induced rapid dissolution of cellulose at low temperatures. Macromolecules 41(23):9345–9351

Cai J, Liu S, Feng J, Kimura S, Wada M, Kuga S, Zhang L (2012) Cellulose–silica nanocomposite aerogels by in situ formation of silica in cellulose gel. Angew Chem 124(9):2118–2121

Caruso R, Schattka J (2000) Cellulose acetate templates for porous inorganic network fabrication. Adv Mater 12(24):1921–1923

Chang C, Duan B, Zhang L (2009) Fabrication and characterization of novel macroporous cellulose–alginate hydrogels. Polymer 50(23):5467–5473

Chang C, Chen S, Zhang L (2011a) Novel hydrogels prepared via direct dissolution of chitin at low temperature: structure and biocompatibility. J Mater Chem 21(11):3865–3871

Chang C, He M, Zhou J, Zhang L (2011b) Swelling behaviors of pH-and salt-responsive cellulose-based hydrogels. Macromolecules 44(6):1642–1648

Chen M, Wang L-Y, Han J-T, Zhang J-Y, Li Z-Y, Qian D-J (2006) Preparation and study of polyacryamide-stabilized silver nanoparticles through a one-pot process. J Phys Chem B 110(23):11224–11231

Chen M, Feng Y-G, Wang X, Li T-C, Zhang J-Y, Qian D-J (2007) Silver nanoparticles capped by oleylamine: formation, growth, and self-organization. Langmuir 23(10):5296–5304

Chen X, Shen S, Guo L, Mao SS (2010) Semiconductor-based photocatalytic hydrogen generation. Chem Rev 110(11):6503–6570

Dankovich TA, Gray DG (2011) Bactericidal paper impregnated with silver nanoparticles for point-of-use water treatment. Environ Sci Technol 45(5):1992–1998. doi:10.1021/es103302t

Dinh C-T, Nguyen T-D, Kleitz F, Do T-O (2011) Large-scale synthesis of uniform silver orthophosphate colloidal nanocrystals exhibiting high visible light photocatalytic activity. Chem Commun 47(27):7797–7799

Ge M, Zhu N, Zhao Y, Li J, Liu L (2012) Sunlight-assisted degradation of dye pollutants in Ag_3PO_4 suspension. Ind Eng Chem Res 51(14):5167–5173

Han C, Pelaez M, Likodimos V, Kontos AG, Falaras P, O'Shea K, Dionysiou DD (2011) Innovative visible light-activated sulfur doped TiO_2 films for water treatment. Appl Catal B 107(1):77–87

Hoffmann MR, Martin ST, Choi W, Bahnemann DW (1995) Environmental applications of semiconductor photocatalysis. Chem Rev 95(1):69–96

Hu H, Jiao Z, Yu H, Lu G, Ye J, Bi Y (2013) Facile synthesis of tetrahedral Ag_3PO_4 submicro-crystals with enhanced photocatalytic properties. J Mater Chem A 1(7):2387–2390

Isogai A, Usuda M, Kato T, Uryu T, Atalla RH (1989) Solid-state CP/MAS carbon-13 NMR study of cellulose polymorphs. Macromolecules 22(7):3168–3172

Jeon J, Lee H-B-R, Bao Z (2013) Flexible wireless temperature sensors based on Ni microparticle-filled binary polymer composites. Adv Mater 25(6):850–855. doi:10.1002/adma.201204082

Khan SU, Al-Shahry M, Ingler WB (2002) Efficient photochemical water splitting by a chemically modified n-TiO_2. Science 297(5590):2243–2245

Kim G-M, Lee S-M, Michler G, Roggendorf H, Gosele U, Knez M (2008) Nanostructured pure anatase titania tubes replicated from electrospun polymer fiber templates by atomic layer deposition. Chem Mater 20(9):3085–3091

Kotel'nikova N, Demidov V, Wegener G, Windeisen E (2003) Mechanisms of diffusion-reduction interaction of microcrystalline cellulose and silver ions. Russ J Gen Chem 73(3):427–433

Kudo A, Ueda K, Kato H, Mikami I (1998) Photocatalytic O2 evolution under visible light irradiation on BiVO4 in aqueous AgNO3 solution. Catal Lett 53(3–4):229–230

Linsebigler AL, Lu G, Yates JT Jr (1995) Photocatalysis on TiO_2 surfaces: principles, mechanisms, and selected results. Chem Rev 95(3):735–758

Liu S, Zhang L, Zhou J, Xiang J, Sun J, Guan J (2008) Fiberlike Fe_2O_3 macroporous nanomaterials fabricated by calcinating regenerate cellulose composite fibers. Chem Mater 20(11):3623–3628

Liu S, Ke D, Zeng J, Zhou J, Peng T, Zhang L (2011a) Construction of inorganic nanoparticles by micro-nano-porous structure of cellulose matrix. Cellulose 18(4):945–956

Liu S, Zhou J, Zhang L (2011b) In situ synthesis of plate-like Fe_2O_3 nanoparticles in porous cellulose films with obvious magnetic anisotropy. Cellulose 18(3):663–673

Luo X, Liu S, Zhou J, Zhang L (2009) In situ synthesis of Fe_3O_4/cellulose microspheres with magnetic-induced protein delivery. J Mater Chem 19(21):3538–3545

Maeda K, Teramura K, Lu D, Takata T, Saito N, Inoue Y, Domen K (2006) Photocatalyst releasing hydrogen from water. Nature 440(7082):295

Mor GK, Shankar K, Paulose M, Varghese OK, Grimes CA (2006) Use of highly-ordered TiO2 nanotube arrays in dye-sensitized solar cells. Nano Lett 6(2):215–218

Murray B, Li Q, Newberg J, Menke E, Hemminger J, Penner R (2005) Shape-and size-selective electrochemical synthesis of dispersed silver (I) oxide colloids. Nano Lett 5(11):2319–2324

Nakayama A, Kakugo A, Gong JP, Osada Y, Takai M, Erata T, Kawano S (2004) High mechanical strength double-network hydrogel with bacterial cellulose. Adv Funct Mater 14(11):1124–1128

Nguyen T-D, Dinh C-T, Do T-O (2009) Monodisperse samarium and cerium orthovanadate nanocrystals and metal oxidation states on the nanocrystal surface. Langmuir 25(18):11142–11148

O'regan B, Grfitzeli M (1991) A low-cost, high-efficiency solar cell based on dye-sensitized. Nature 353:737–740

Patterson A (1939) The Scherrer formula for X-ray particle size determination. Phys Rev 56(10):978

Pinto RJ, Marques PA, Barros-Timmons AM, Trindade T, Neto CP (2008) Novel SiO_2/cellulose nanocomposites obtained by in situ synthesis and via polyelectrolytes assembly. Compos Sci Technol 68(3):1088–1093

Qi H, Chang C, Zhang L (2009) Properties and applications of biodegradable transparent and photoluminescent cellulose films prepared via a green process. Green Chem 11(2):177–184

Sehaqui H, Liu A, Zhou Q, Berglund LA (2010) Fast preparation procedure for large, flat cellulose and cellulose/inorganic nanopaper structures. Biomacromolecules 11(9):2195–2198

Soltani Z, Ziaie F, Ghaffari M, Afarideh H, Ehsani M (2013) Mechanical and thermal properties and morphological studies of 10 MeV electron beam irradiated LDPE/hydroxyapatite nano-composite. Radiat Phys Chem 83:79–85

Tang J, Zou Z, Ye J (2004) Efficient photocatalytic decomposition of organic contaminants over CaBi2O4 under visible-light irradiation. Angew Chem Int Ed 43(34):4463–4466

Thomas M, Ghosh S, George K (2002) Characterisation of nanostructured silver orthophosphate. Mater Lett 56(4):386–392

Tokunaga S, Kato H, Kudo A (2001) Selective preparation of monoclinic and tetragonal $BiVO_4$ with scheelite structure and their photocatalytic properties. Chem Mater 13(12):4624–4628

Tsuji I, Kato H, Kudo A (2005) Visible-light-induced h2 evolution from an aqueous solution containing sulfide and sulfite over a ZnS–CuInS2–AgInS2 solid-solution photocatalyst. Angew Chem 117(23):3631–3634

Wang H, Bai Y, Yang J, Lang X, Li J, Guo L (2012) A facile way to rejuvenate Ag_3PO_4 as a recyclable highly efficient photocatalyst. Chem Eur J 18(18):5524–5529

Xiang Y, Peng Z, Chen D (2006) A new polymer/clay nanocomposite hydrogel with improved response rate and tensile mechanical properties. Eur Polym J 42(9):2125–2132

Yang H, Wu X-L, Cao M-H, Guo Y-G (2009) Solvothermal synthesis of $LiFePO_4$ hierarchically dumbbell-like microstructures by nanoplate self-assembly and their application as a cathode material in lithium-ion batteries. J Phys Chem C 113(8):3345–3351

Yi Z, Ye J, Kikugawa N, Kako T, Ouyang S, Stuart-Williams H, Yang H, Cao J, Luo W, Li Z (2010) An orthophosphate semiconductor with photooxidation properties under visible-light irradiation. Nat Mater 9(7):559–564

Yu D-H, Yu X, Wang C, Liu X-C, Xing Y (2012) Synthesis of natural cellulose-templated TiO_2/Ag nanosponge composites and photocatalytic properties. ACS Appl Mater Interfaces 4(5):2781–2787

Zhang H, Wang G, Chen D, Lv X, Li J (2008) Tuning photoelectrochemical performances of Ag − TiO_2 nanocomposites via reduction/oxidation of Ag. Chem Mater 20(20):6543–6549

Zhao Z, Jiao X, Chen D (2009) Preparation of TiO_2 aerogels by a sol-gel combined solvothermal route. J Mater Chem 19(19):3078–3083

Zheng R, Lin L, Xie J, Zhu Y, Xie Y (2008) State of doped phosphorus and its influence on the physicochemical and photocatalytic properties of P-doped titania. J Phys Chem C 112(39):15502–15509